Calibration Experiment of All-sky Electrostatic Analyzer

MIYAKE Wataru and YAMAZAKI Atsushi

Electrostatic analyzers have been widely used for measuring the energy and incident angle distribution of space plasma on board the spacecraft. The measurement enables us to derive the flow velocity, density, and temperature of plasma, to detect the large-scale disturbances in space, and to forecast the space weather. An electrostatic analyzer with all-sky field of view has been developed for the L5mission and the proto-type model is calibrated by a ground facility. The results demonstrate a fair agreement with the numerical model calculations and its capability of the space plasma measurement on board 3-axis stabilized spacecraft such as the L5 mission.

Keywords
L5 mission, Solar wind plasma, Electrostatic analyzer

1 Introduction

Electrostatic analyzers have commonly been used as plasma measuring instruments aboard satellites to measure the energy distribution and three-dimensional velocity distribution of space plasma. The electrostatic analyzer measures the E/q (energy per charge) of particles using the unique kinetic characteristic of charged particles in an electrostatic field. The measured energy of space plasma (ions and electrons) around a satellite and the incident angle distribution obtained by the analyzer are used to calculate the plasma flow velocity, density, and temperature and to detect large-scale space disturbances. The information obtained on the plasma structure and propagation is used to forecast space weather. Further, the micro-scale velocity distribution functions of ions and electrons provide us with a better understanding of particle acceleration, wave-particle interactions, and the propagation of accelerated particles in space plasma. Moreover, by adding [1] a TOF (Time-Of-Flight) velocity analysis function to the final stage of the electrostatic analyzer, it will be possible to identify individual species of ions (such as H^+, He^{++}, and O^+).

In an electrostatic analyzer, two opposing electrodes generate a potential difference through which charged particles are passed. These analyzers are categorized in accordance with the structure of the electrodes, and include the parallel plate type, the concentric cylinder type, and the spherical type. The spherical electrostatic analyzer has only one inlet, which particles enter from various angles. Since the exit position of a particle varies according to its incident angle, detecting the exit locations enables the simultaneous measurement of the incident angle distribution (one-dimensional) and the energy distribution. Therefore, when a satellite mounted with a spherical electrostatic analyzer rotates about its spin axis, the analyzer is able to perform three-dimensional velocity distribution measurement. Because of this advantage, spherical electrostatic analyzers are often installed on satellites for space plasma measurement. To date, the ISEE [2]-[5], GEOS [6], AMPTE [7][8],

Giott [9], Ulysess [10], and Galileo [11] have carried onboard spherical electrostatic analyzers. However, even a spherical analyzer with a wide angle of visibility still has a range of dead angles, and its analytical characteristic will therefore vary depending on the line of sight. This drawback was solved in the so-called "top-hat" electrostatic analyzer [12][13]. Its axially perfect symmetrical shape ensures uniform analytical characteristic over a field of view of 2π rad.

In Japan, three analyzers were designed for the observation of solar wind plasmas and mounted on satellites. Two were 270° spherical electrostatic analyzers [14][15], and the third was a top-hat electrostatic analyzer [16]. However, these analyzers were all mounted on satellites with spin-stabilized attitude control and thus featured only one-dimensional angular resolution. By positioning the one-dimensional field of view on a plane that partially includes the satellite's rotation axis, the satellite's rotation and the one-dimensional angular resolution are combined to enable the measurement of angle distributions of two orthogonal components, and also to provide a three-dimensional velocity distribution function when coupled with measurement of energy distribution.

With a satellite using three-axis attitude control, in theory it is not possible to perform three-dimensional velocity distribution measurement using the above-mentioned three analyzers. Three-axis control is expected to be adopted for the L5 mission [17] aimed at imaging CME in interplanetary space and activity on the sun's surface. In such a satellite, innovative measures are required to widen the field of view of the measuring instrument. One method of establishing such an electrostatic sweep is to install electrostatic deflecting electrodes at the entrance section of the analyzer. In the WIND satellite, the collimator section of the onboard top-hat electrostatic analyzer was provided with deflecting electrodes to achieve a field of view greater than ±45 degrees [18]. Figure 1 (a) is a schematic diagram of this type of analyzer. The arrows in the diagram indicate the traveling directions of particles that enter and exit the instrument. The field of view is the circular area of approximately ±45 degrees from both sides of the plane (indicated by a dotted line in the diagram) perpendicular to the analyzer's symmetry axis. As a result, the satellite body can easily interfere with the analyzer's field of view. Thus for maximum performance, this type of analyzer must be installed at the tip of an extended element, such as a boom.

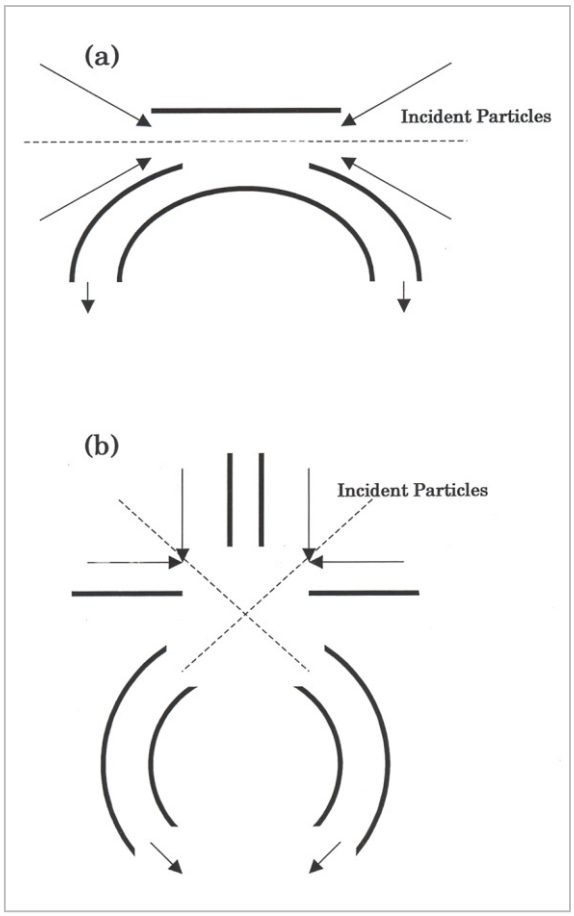

Fig.1 *Cross-sectional diagram and schematic of incident and exit particles of top-hat electrostatic analyzer (a) and newly developed electrostatic analyzer prototype (b)*

On the other hand, a bottle-type analyzer offers a full-sky field of view (2π str), conducting its sweep by opening and closing a conical surface with a field of view formed at an angle of 45 degrees from the analyzer axis. Fig.1 (b) is a schematic diagram of this type of analyzer. Unlike the top-hat analyzer, this ana-

lyzer can be mounted directly on the outer surface of a satellite, a major advantage.

To examine this analyzer in detail, we obtained a potential distribution based on specific shape and electrode arrangement, and used a numerical model to calculate the traveling paths of a large number of particles within the analyzer [19]. This investigation revealed favorable analyzer performance. Accordingly, this paper introduces a prototype electrostatic analyzer with a full-sky field-of-view sweep function, designed for installation on a satellite such as the L5 mission featuring three-axis control, and also discusses the results of an experiment we conducted to evaluate basic analyzer performance, using a specific ion-beam charged-particle calibration device [20].

2 Outline of the prototype analyzer

A cross section of the prototype analyzer is shown in Fig.2. In this figure, the prototype analyzer has been rotated 90 degrees from that shown in Fig.1 (b). The analyzer is made mainly of aluminum and constitutes the conductor section (blue shaded area in the diagram), and the deflection plates and energy analyzer electrodes are electrically insulated by UPIMOL (red shaded area in the diagram).

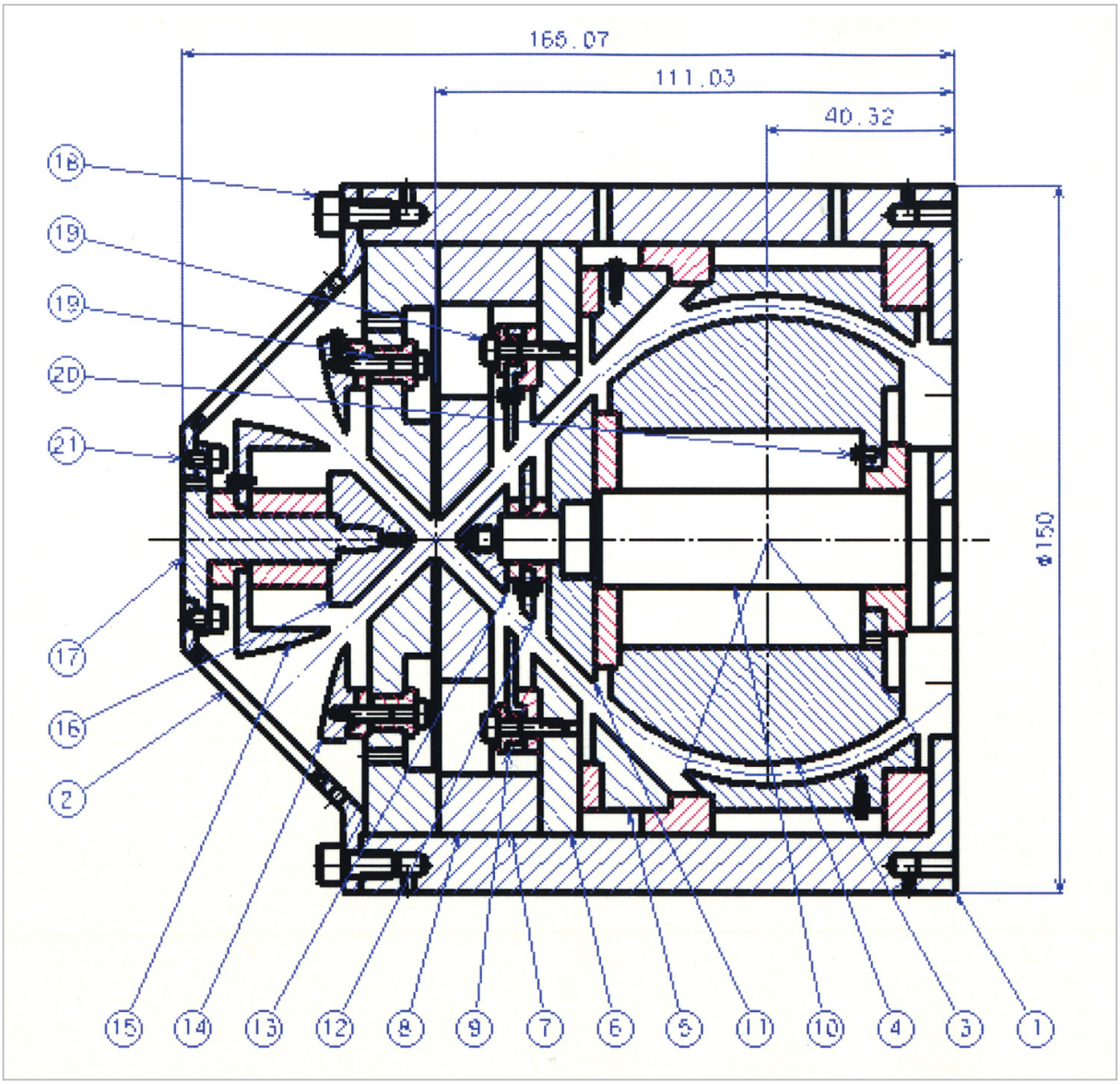

Fig.2 *Cross-sectional view of prototype analyzer*

Since the prototype was produced to test the analyzer's basic functions in a ground facility, we designed it without taking weight, impact resistance, other mechanical characteristic, or thermal characteristic into consideration. We also determined the shape with a main focus on achieving dimensional precision without the use of special assembly techniques. We ensured an accuracy of 5 ±0.05 mm for the passage width along the charged particle channels. The shape of this prototype analyzer was determined based on the results of numerical calculation, and the size [19] was optimized for the measurement of solar wind electrons aboard the L5 mission. Although some have expressed the opinion that a larger device would be more suitable for measurement of solar wind ions (this will be discussed later in detail), we determined the size of the prototype component in view of the uniform diameter of the ion beams generated by the charged-particle calibration device [20] used in our experiment. A larger instrument would render quantitative evaluation difficult. In other words, the prototype was produced to assess basic performance with respect to the analyzer shape; the optimal size will be investigated based on these results and in accordance with the scaling law of charged particle paths in an electrostatic potential field.

The prototype analyzer consists primarily of three types of electrodes: electrostatic deflecting electrodes for line-of-sight scanning, limiter electrodes to adjust sensitivity, and spherical electrodes to analyze particle energy. Electrostatic potentials created by an external power supply are applied to the electrodes. The analyzer is in cylindrical symmetry. Particles enter the analyzer from the upper left and lower left and move toward the center of the X shape in the diagram. Particles pass through a mesh section that prevents the analyzer's internal potential from leaking to the outside. Particles then travel between the two facing deflecting electrodes each featuring a cuneiform cross section. By applying a potential to these facing deflection electrodes, the analyzer generates an electrical field between the electrodes and bends the paths of incident particles to freely deflect the line of sight.

After particles pass the center of the X, they travel past the thin annular limiter electrodes, which serve as the "diaphragm" for sensitivity adjustment. Application of a voltage to the limiter electrodes reduces the number of passing particles, enabling the measurement of a high particle flux. Since the dynamic range (number of particles measured per given period) of the particle detector in the final stage is limited, this function was adopted to expand the dynamic range of the measuring instrument and to enable measurement of both extremely small and very large particle flux.

Particles are then led to the spherical electrostatic analyzer section. The radii of the outer and inner spheres are 52.5 mm and 47.5 mm, respectively. A potential difference is applied to the space between the two spheres, so particles travel in a near-circular orbit. Particles with energies that are too great relative to the applied potential difference travel almost linearly, strike the outer sphere, and are unable to exit. Orbits of particles with very low energies are bent substantially; these particles collide with the inner sphere, and are similarly blocked. As a result, only particles at the appropriate energy level exit the spherical analyzer.

Particles passing through the spherical analyzer reach the exit located at the right end, where the detector converts them to electric signals, which are detected as a pulse count. In our experiment we used a microchannel plate (MCP) [21], a type of secondary electron amplifying tube, as a detector. Particles fly around the analyzer in all directions and at all energy levels, but only particles with incident angles and energy levels satisfying certain conditions relative to the potential applied to the electrodes reach the final-stage detector. All other charged particles collide against the passage walls before reaching the final stage. Changing the combination of voltages applied to the individual electrodes and examining the number of passing particles provides informa-

tion on the angle-energy distribution of the charged particles within the analyzer. For further details, refer to the investigation based on the numerical model calculations [19].

3 Outline of test equipment and test procedures

Prototype performance was investigated with a charged-particle calibration device [20]. This device produced parallel N_2^+ ion beams at a uniform energy level within a vacuum chamber, albeit in conditions quite different from those of actual plasma in space. Since the ion beam generator was a particularly elaborate device, we did not vary its energy level or direction of radiation, but instead maintained these at constant values. Instead, to study angular characteristic, the analyzer was placed on a vacuum gimbals (rotating platform) with two orthogonal axes, and was rotated to vary the direction at which the beam entered the analyzer. To investigate energy characteristic, on the other hand, the voltages applied to the electrodes inside the analyzer were varied in fine increments. Figure 3 shows the analyzer setup on the dual-axis vacuum gimbals inside the vacuum chamber. Ions were directed from left to right in the photo.

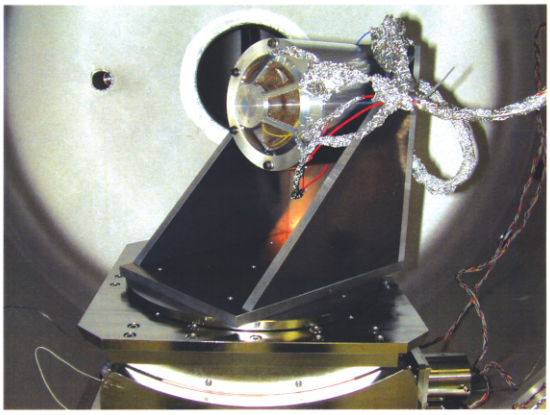

Fig.3 *Prototype analyzer on dual-axis vacuum gimbals (rotating platform) inside vacuum chamber*

All devices used to measure analyzer characteristic were controlled from a single personal computer via GPIB communication. These devices included the following:

* Analog voltage power supply unit, providing control voltage to the ion-beam control equipment
* Multiplexer and multimeter to monitor ion beam current and voltage
* Controller for gimbals control
* Multiplexer and multimeter to monitor power applied to the analyzer and output voltage
* Detector output pulse counter
* Ionization vacuum gauge (for monitoring of degree of vacuum)

Figure 4 shows the control screen displayed on the PC. To enable independent control, we included separate control panels (on the right side of the screen) within the application. The sample screen shows the main panel for automatic control sweep measurement and the sweep control panel. To check the analyzer characteristic for a selected parameter, all other parameters were fixed, and an automatic sweep was conducted for the selected parameter while output pulse number was tallied, enabling the smooth acquisition of data. The sweep measurement items can be divided roughly into the following three groups:

(1) Measurements related to output ion beams (voltage/current sweep)
(2) Measurements related to analyzer direction (incident angle sweep)
(3) Measurements of voltage applied to analyzer (energy, angle of visibility, sensitivity sweep)

Measurements of the first type were conducted by applying a control voltage to the ion beam control device from the analog voltage output device controlled by the GPIB communication. For type 2 measurement, a sweep was conducted by rotating the gimbals inside the chamber. For type 3 measurement, the voltage applied to the observation equipment was swept while the power supply voltage was controlled directly by the GPIB.

In the experiment, the control panels (see Fig.4) on the PC display were operated according to the flow chart shown in Fig.5.

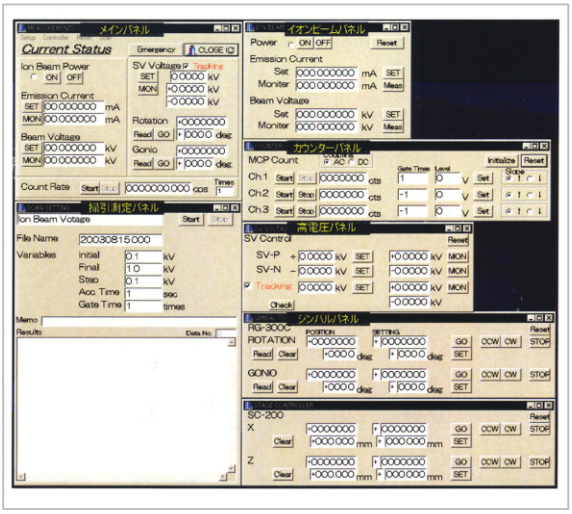

Fig.4 *Control panels on PC screen*

First, a sweep item was selected, and all other parameters were fixed using the main panel.

Next, using the sweep control panel, the initial value, final value, and step value, as well as the observation time at each measuring point, were set. The Scan Start button was clicked to start sweep measurement. At each point, measurement began when the device stabilized, one second after termination of the parameter sweep. After the measurement was completed at each point, the result was output and displayed in the space below the sweep control panel. After the measurement was completed at the final sweep point, the data was output as a file for analysis.

4 Analyzer characteristic

4.1 Energy-angle characteristic

Since the analyzer was axially symmetrical, dependency on elongation of the axis should be investigated. Here, the in-plane orthogonal to this axis was defined as having an elevation angle of 0 degrees, and the leftward plane parallel to the axis in Fig.2 was set as 90 degrees. When the deflecting electrodes for the field-of view sweep were grounded (i.e., when the deflection was 0), incident particles would reach the entrance of the spherical energy analyzer centering around the elevation angle of 45 degrees. By rotating and fixing the gimbals at a certain elevation angle

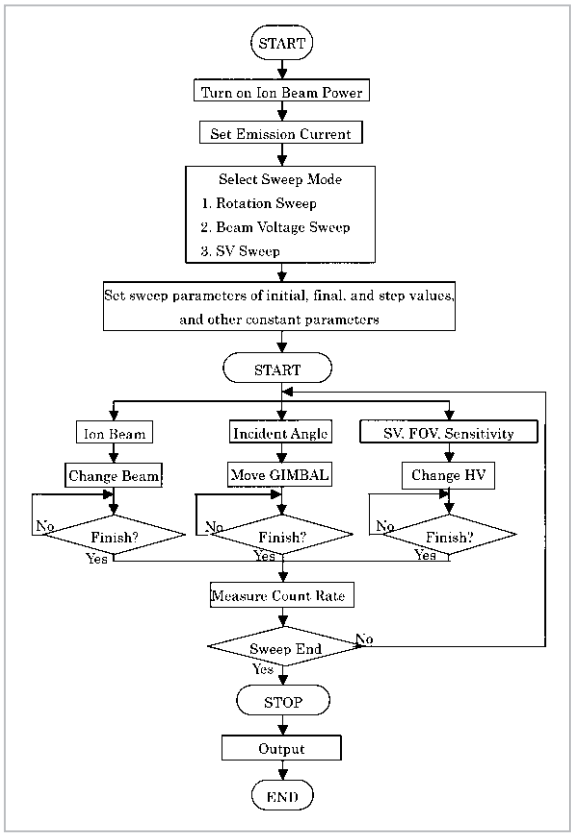

Fig.5 *Measurement flow chart*

and incrementally varying the potential (sweep voltage, or SV) applied to the inner and outer spherical electrodes of the spherical analyzer, we were able to count the number of transmitted particles per unit time in each step. In this experiment, a positive potential was applied to the outer sphere, and a negative potential of the same degree was applied to the inner sphere. Next, we moved the gimbals slightly to change its fixed elevation angle and conducted the SV sweep again over the same range. Repeating this process yielded the energy-angle characteristic near 45 degrees shown in Fig.6. In the graph, the maximum transmission rate percentage (particle count) was assigned the value of 100%, contour lines were also plotted at 80%, 60%, 40%, and 20%.

Charged particles featuring the same ratio of kinetic to potential energy (i.e., the same potential distribution) followed the same paths in the electrostatic field, in accordance with the scaling law. Therefore, the degree of particle energy relative to SV was indicated on the

horizontal axis. When ±100 V was applied to both the outer and inner spheres, particles with an energy level of 850 eV to 1,000 eV passed through. This SV value is proportionally related to the energy value of transmitted particles. In other words, particles of approximately 9 * SV [eV] relative to the applied ±SV will pass through the analyzer and be detected by the detector.

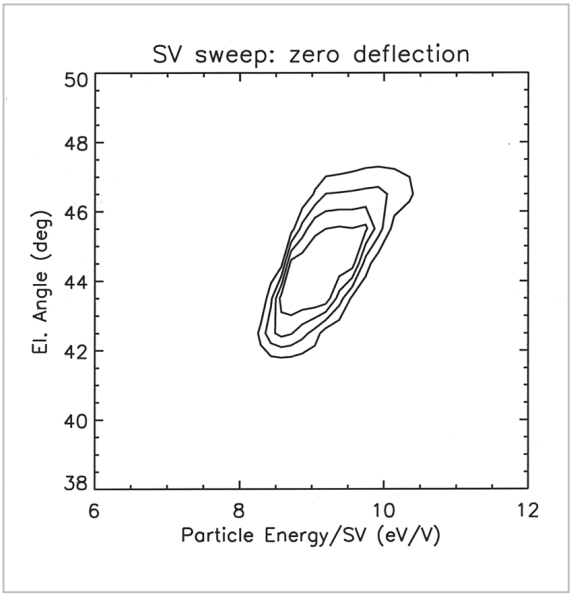

Fig.6 *Energy-angle characteristic (measured value) at an elevation angle approaching 45 degrees*

The energy resolution and angular resolution are defined as half-value widths of the integral distribution in the vertical and horizontal directions, as seen in Fig.6. Since the above scaling law applies to the horizontal axis, the resolutions can be defined as the ratio to the median of the half-value widths. In this case, the energy resolution is approximately ±7%, and the angle resolution is approximately ±1.8 degrees.

Figure 7 shows the energy-angle characteristic of the analyzer obtained based on numerical model calculations [19]. This characteristic is expressed in the same format as that used in Fig.6, and agrees well to the graph in Fig.6, indicating that this characteristic was as estimated using the numerical calculations. Detailed comparison, however, revealed a slightly wider spread in both energy and angle distributions. We suspect that this was attributable to limitations posed by the singularity of energy and the parallelism of the ion beams used in the experiment, in addition to manufacturing and assembly deviations, but we could not determine the exact cause. Nevertheless, we believe that the close correspondence between predicted and actual results supports the practical application of the analyzer under study.

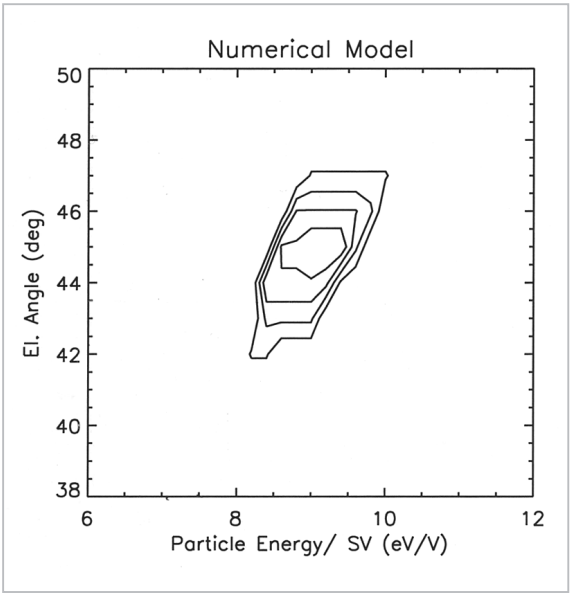

Fig.7 *Energy-angle characteristic (model calculation) at an elevation angle approaching 45 degrees*

The absolute sensitivity of an analyzer is referred to as the G factor, and it indicates the ratio of transmission energy width multiplied by the transmission solid angle to the product of opening area and center transmission energy. In other words, integration of the transmission counts indicated by the contour lines in Figs. 6 and 7 by energy and angle, in addition to integration of the directions orthogonal to the elevation angles, will yield the G factor, provided that the incident particle flux is known. The number of particles C (/sec) per unit time measured at the center transmission energy E and the differential flux F (/cm^2 str keV sec) displays the following relation: $C = F(E) \cdot G \cdot E \cdot \varepsilon$. Here, ε is the detection efficiency of the detector and G is the G factor. In our experiment, we could not measure the

absolute ion beam flux with sufficiently high precision; therefore, we were unable to obtain the G factor. However, since the energy-angle characteristic matches that of the numerical model calculations, it is safe to assume the applicability of the G factor value obtained in these calculations.

In both Figs. 6 and 7, coupling is seen between particle energy/SV and elevation angle (EL), and skewing [22] (distortion) is generated. This skewing occurs when the bending angle (angle of deflection of particle paths inside the spherical analyzer) is smaller than 180 degrees [23]. Particles with high energies are not easily deflected and thus they are able to reach the exits near the outer sphere. Therefore, when the incident angle is directed outward (from the inner sphere toward the outer sphere), particles move even farther away from the centers of the concentric spheres at the exits, collide against the outer sphere, and are blocked from passing through the analyzer. If the incident angle is directed inward, on the other hand, particles tend to deflect toward the center (toward the inner sphere), thus mitigating the effect of their higher energies and allowing them to pass through. With particles at lower energies, the opposite phenomena are seen. As a result, skewing is generated between energy and incident angle, as shown in Figs. 6 and 7.

When processing measurement data for actual space plasma, this skewing and slight variation in transmission rate can be ignored in most cases. In other words, in the case of an analyzer with an energy resolution of δ% and angular resolution of α degrees, uniform transmission is assumed in the area within $\pm\delta$% relative to the center energy corresponding to the applied SV and within $\pm\alpha$ degrees from the direction in which the analyzer faces. This area corresponds to that of the rectangle in Figs. 6 and 7. Outside this area, transmission is considered to be zero. This approximation is valid when the energy-angle distribution of measured plasma is sufficiently large in relation to δ and α. For example, when the temperature of plasma is extremely low, the analyzer must have low values for δ and α in order to obtain accurate measurements.

4.2 Field-of-view deflection

We examined the relationship between the deflection voltage (Vdef) and elevation angle (El. angle) observed when an electric potential is applied to the deflecting electrodes for a field-of-view sweep. Figure 8 shows the results of this experiment, and Fig.9 indicates the results of the calculations using the numerical model. As described in (4.1), the particle energy and the voltage applied to the electrodes are governed by the scaling law; the ratio of deflection voltage to particle energy is shown on the vertical axis. In the experiment, a positive potential was applied to one of the two deflection electrodes and the other electrode was grounded (zero potential). In the diagram, those ratios of the positive side of the vertical axis indicate the application of a positive voltage to the electrode, which was near the symmetry axis and cylindrical in shape (as seen in Fig.2), while those ratios of the negative side of the vertical axis indicate the application of positive voltage to the disc-shaped electrode, for easier understanding. This figure shows an overall view of the field-of-view sweep characteristic. At the zero position on the vertical axis, both electrodes were grounded.

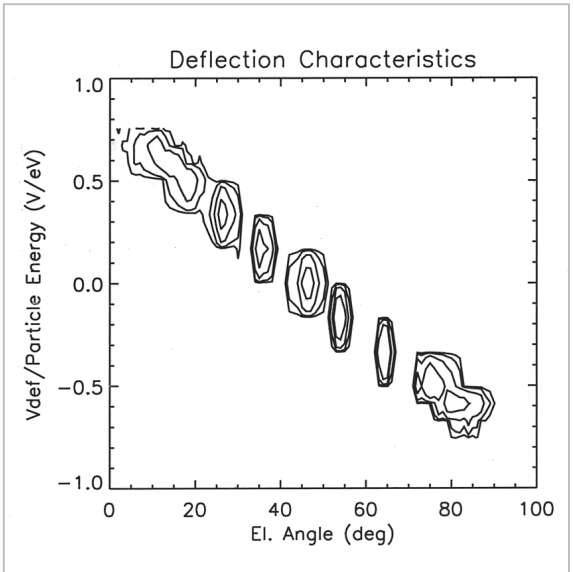

Fig.8 *Field-of-view deflection (measured value)*

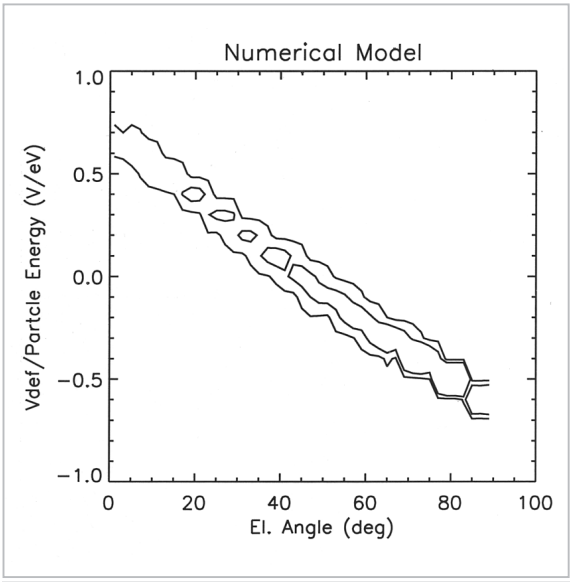

Fig.9 *Field-of-view deflection (model calculation)*

In Fig.8, the contour lines are discontinuous, but this was attributable to the large scattering of measurement points. In reality, the contour lines would be smooth. In Fig.9, stepped changes can be seen, but these were due to the finite number of numerical calculation points. In both graphs, a near-linear relation can be observed between the applied value and field-of-view deflection angle. Furthermore, the entire field of view is covered with a maximum voltage of 70 % to 80 % of the particle energy.

Although the electrostatic deflection electrodes appear to be symmetrical with respect to the conical 45-degree surface, a three-dimensional view indicates that the deflecting electrode near the axis is almost cylindrical in shape, and that the other deflection electrode is nearly flat. Therefore, the formed potential structure acts as a convex mirror when a voltage is applied to the cylindrical electrode near the symmetry axis, and as a concave mirror when a voltage is applied to the disc-shaped deflection electrode. Therefore, parallel incident particles diffuse in the former case (< 45 degrees), and they converge in the latter case (> 45 degrees).

Due to these effects of diffusion and convergence, the percentage of transmission is higher for incident particles with a large elevation angle than for incident particles with a small elevation angle. When a voltage was applied to the flat electrode (> 45 degrees), the deflection was slightly higher (same degree of deflection observed at a low voltage) than when a voltage was applied to the cylindrical electrode near the symmetry axis (< 45 degrees). We suspect that the slight variation in deflection may be linked to the potential structure; i.e., whether it promoted diffusion or convergence.

4.3 Limiter characteristic

Last, we investigated the sensitivity adjustment function by applying voltage to the annular limiter electrodes installed between the field-of-view sweep electrostatic deflecting electrodes and the spherical electrodes for energy analysis. The results are shown in Fig.10. The graph shows the integration (sum) over angles in the data obtained in SV sweeping at varied incident angles. The solid line corresponds to the data in Fig.6, and the voltage applied to the limiter was zero. The dashed line indicates the data obtained by applying a voltage equivalent to 80 % of particle energy, while the dotted line shows the data acquired by applying a voltage equivalent to 90 % of particle energy. Figure 11 shows the results of the corresponding numerical model calculations.

The measured values and the model calculation results matched closely, thus indicating the feasibility of controlling an approximately tenfold variation in sensitivity, as we expected. Application of voltage to the limiter electrodes not only reduced the number of transmitted particles but also increased the transmitted particle energy/SV value slightly, as predicted under the numerical model. This demonstrated that this type of limiter not only hinders the transmission of particles with energies lower than the applied voltage, but that it also modifies the paths of the transmitted particles, performing its limiting function in combination with the energy-incident angle characteristic of the spherical analyzer in the later stage. Therefore, even an applied voltage

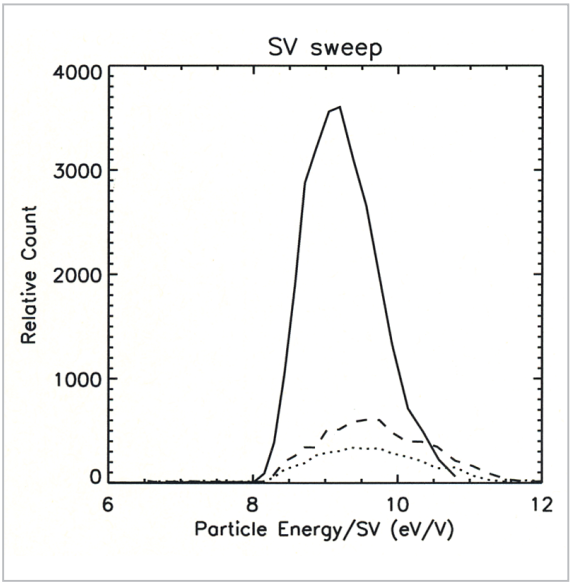

Fig.10 *Limiter characteristic (measured values).*

Solid, dashed, and dotted lines represent data obtained with the limiter voltage/particle energy values of 0.0, 0.8, and 0.9 (V/eV), respectively.

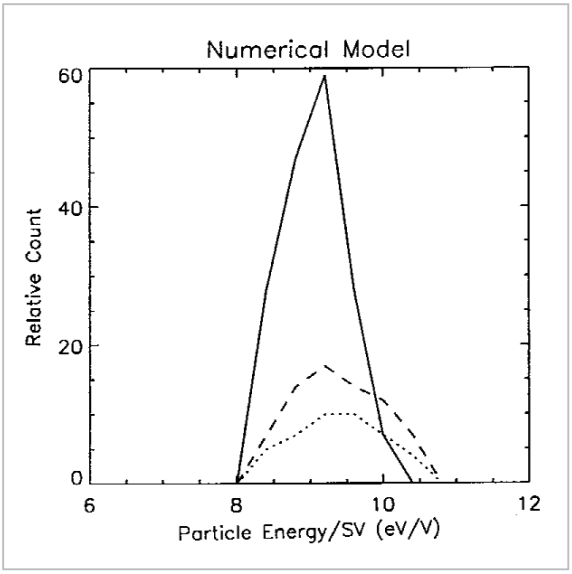

Fig.11 *Limiter characteristic (model calculations).*

Solid, dashed and dotted lines represent data obtained under the same conditions as those in Fig.10.

of approximately 80% of particle energy/q will result in a noticeable decrease in sensitivity.

Although the limiter electrodes were arranged as if the inside and outside of the electrodes would provide about the same function and form an equipotential surface nearly perpendicular to the direction of particle motion shown in Fig.2, the convergence/diffusion lens effects were the same as those seen with the field-of-view sweep electrostatic deflecting electrodes, converging particle beams that were parallel before entering the spherical analyzer to a focal point, as predicted particle paths under the numerical model. Due to the three-dimensional effect, the focal point is slightly displaced from the center, toward the exterior. Therefore, particles entering the spherical analyzer became diffused particle beams emitted from a focal point closer to the outer sphere. This means that the incident particles followed a path from the outside toward the inside of the outer sphere. Therefore, similar to the skewing of the energy-incident angle of the spherical analyzer explained in (4.1), the transmission of particles directed inward features a lower SV value (that is, a higher particle energy/SV) and minimal bending. We believe that this caused the particle energy/SV to increase slightly, as indicated by the dashed and dotted lines in Figs. 10 and 11.

5 Summary and discussion

The following summarizes the main characteristic of the prototype analyzer.

1) The energy resolution and incident angular resolution were ±7 % and ±1.8 degrees, respectively, and the center transmission energy/analyzer applied voltage was 9 (eV/V).

2) By applying a maximum voltage of 70 % to 80 of the particle energy/q to the electrostatic deflecting electrodes, the analyzer achieved a field-of-view sweep of ±45 degrees for a full-sky field of view (2π str).

3) By applying a voltage of 80 % to 90 of the particle energy/q to the limiter, it is possible to reduce sensitivity to approximately 10 % of the original value.

These values were very close to those estimated based on the calculation results of the numerical model, although slight deviations were noted. It was thus confirmed that the prototype analyzer fulfilled its designed func-

tions. The validity of the numerical model produced prior to design was also verified, indicating that the model may be used for detailed investigation and design analysis in the future. Although the instrument's sensitivity (G factor) was not measured directly in our experiment, given the fact that the above energy-incident angle characteristic corresponded to the model calculation results, we concluded that the actual G factor would also correspond to the predicted value under the numerical model. Although a number of aspects remain to be examined prior to installation on a satellite—such as vibration and impact resistance mechanical characteristic, and thermal characteristic in a vacuum—development of our prototype represents a major step forward in the development of a plasma measurement instrument with a full-sky field of view to be mounted on a satellite with three-axis control.

Next we will discuss solar wind plasma measurement in the context of the L5 mission. Solar wind electrons consist of isotropic thermal cores of up to approximately 30 eV and high-energy tail halos elongated along the magnetic field lines to several hundred eV [24]. Further, electrons accelerated during the generation of solar flares propagate at energies of several hundred eV or more, mainly in the direction of the magnetic field lines [25].

For measurement of thermal cores and halos of solar wind electrons requiring a field of view in nearly all directions (4π str), installation of two measuring instruments on opposite sides of a satellite may prove effective. The full-sky field of view is limited from 70 % to 80 % of the maximum output (several keV) of the high-voltage sweep power supply, but maximum measurement energy can be obtained in the distribution along the 45-degree cone. In the case of electrons, the velocity distribution is expected to be dependent on the pitch angle relative to the magnetic field lines; therefore, when the conical surface and the magnetic field lines are parallel, all pitch angles are covered. For installation on a satellite, it is best to position the analyzer so that the direction of the 45-degree field-of-view center conical surface is aligned with the direction of the Parker spiral (45 degrees east of the sun) toward which interplanetary magnetic fields are, statistically speaking, most frequently pointed. This is expected to cover the angular distribution of electrons accelerated by high-energy flares.

In terms of angular and energy resolution, electron measurement poses no problem, and can be used in the measurement of temperature and unisotropy of thermal electrons. Moreover, the numerical flux of the electrons of the solar wind is a maximum of approximately $10^7/cm^2$ sec str eV. Assuming that the width of the detector anode for azimuth distribution measurement is roughly 30 degrees, the sensitivity (G factor) near the incident angle of 45 degrees is 7.2×10^{-4} cm^2 str eV. From this, the maximum count is estimated to be 10^4 per sec. The maximum total count over the entire detector surface is estimated to be 10^5 per sec.

Solar wind ions consist mainly of protons in supersonic flow. The particle count is high, and these particles are easy to measure with available instrument sensitivities. On the other hand, thermal velocity (several tens of km/sec) is low in relation to bulk velocity (several hundred km/sec). This necessitates higher energy resolution and angular resolution than required to measure ions in the magnetosphere, if we are to secure sufficient energy and angle distributions to perform the velocity distribution function. Thermal proton measurement enables the calculation of basic solar wind macro parameters such as bulk velocity, density, and temperature. These basic parameters are used to detect and identify shock waves, disturbances, CIR, and high-speed streams resulting from CME in solar winds. The variations of these parameters, combined with magnetic field data, are used to detect and identify MHD waves in solar winds, and they provide the basic information concerning pitch angle scattering, heating, and acceleration of ions.

The current energy resolution and angular resolution near an incident angle of 45 degrees are barely sufficient to allow for the proton

velocity distribution function. On the other hand, the proton energy flux reaches an order of nearly 10^8/cm^2 sec str eV. Therefore, based on a G factor with an assumed azimuth width of 1 degree, a count on the order of 10^4/cm^2 sec str eV can be estimated. It is unrealistic to arrange anodes of 1-degree width; widths of 3 to 5 degrees are suspected to be the limit. In addition, due to the widening angle of protons in the solar wind, the total count over the entire detector surface is on the order of 10^5/sec.

Thermal protons have an energy level of approximately 1 keV. Since the velocity of the proton flow is about the same as that of heavy ions in solar winds, observation of this E/q with an analyzer would result in a distribution corresponding to the ionic M/q. In other words, the peak of He^{++} appears at the area where the E/q is twice as high as that of protons (H^+).

Various ions in solar winds not only provide data on the above-mentioned basic solar wind parameters, but also serve two important purposes in observation. As these ions consist of high-energy particles generated and accelerated by shock waves in interplanetary space, their compositions and ionization states offer valuable information on CMEs and other phenomena, enabling in-depth investigation of CMEs and the history of the sun. The highest number of heavy ions in the solar winds are He^{++} ions (α particles), but their density is less than 20 % of that of solar wind protons [26]. The figures for other heavy ions are even lower. Therefore, the three-dimensional velocity distribution function is required only for protons and He^{++}. For other heavy ions, all that is required is an energy distribution based on the integration of angular arrival directions [27].

Ions in a solar wind flow at supersonic speed away from the sun. Therefore, they are more concentrated closer to the sun's direction and as a result there is no need for a full-sky sweep of the electrostatic deflection electrodes from 0 degree to 90 degrees; only the area near the sun needs to be scanned. Therefore, the analyzer must be positioned in such a way that the line of sight of the 45-degree conical surface is aligned toward the sun. To detect particles reflected or accelerated by impulse waves and pick-up ions, the analyzer should be capable of sweeping over certain angles of visibility. In our analyzer, when the high-voltage power supply (maximum output power of 3 kV) was used, the angle of visibility for particles of more than 10 keV was limited to approximately 45 ±15 degrees or less. Since data is obtained in the azimuth direction along the 45-degree conical surface, a certain range can be covered for the measurement of high-energy ions by combining the two of data obtained.

The gain of the MCP used in a detector drops when the output current (count) increases excessively [21]. Although this saturation characteristic depends on the resistance of the MCP, 10^6/sec is the guideline value. The expected lifespan of the MCP is said to depend on the total electric charge discharged from the MCP [21]. Therefore, it is important to take measures to ensure that the application of voltage to the sensitivity adjustment electrodes will not result in an input count exceeding 10^5/sec. Currently this requirement is expected to result in the area near the peak of protons. Therefore, a limiter must be used for measurement in the low energy range, and, in the high-energy range, the maximum sensitivity must be used to measure heavy ions with low flux. This poses no problem, as the limiter voltage requires 80 % to 90 % of the particle energy/q, and the maximum output of the ordinary onboard high-voltage power supply is several keV.

Generally, the energy resolution δE/E of a spherical electrostatic analyzer is approximately proportional to (R2-R1)/(R1+R2), whereas the radii of the inner and outer spheres of the analyzer are R1 and R2, respectively. This means that if the size of the spherical electrodes are increased while maintaining a constant separation between the radii of the two spheres, energy resolution will improve proportionally. Although limited satellite

resources will impose some restrictions in this area, if the center radius can be increased to 100 mm, energy resolution would improve to approximately 1/2. Similarly, the particle energy/SV value may be expected to double, thus enabling measurement within a larger energy range using the same high-voltage power supply. Further, since resolution in the azimuth direction is determined by the positioning resolution of the analyzer, a larger center radius would provide higher angular resolution with the same positional resolution. These points should be taken into consideration when designing the actual ion measurement instruments.

6 Conclusion

Our calibration experiment with the prototype analyzer offers a promising view into the possibility of three-dimensional velocity distribution measurement of plasma with a measuring instrument aboard a satellite featuring three-axis control. In particular we have witnessed major advances in terms of solar wind ions and electron measurement in the context of the L5 mission. We believe that the current design will prove adequate to measure electrons in the solar wind. Future topics in this area include enlargement of the instrument size and the incorporation of identification of ion species via the TOF method. Finally, the analyzer developed here will prove suitable for use not only in the L5 mission but also in the measurement of keV particles in the Earth's magnetosphere.

Acknowledgement

We would like to express our sincere thanks to Mr. Junichi Komuro at the Science and Technology Information Group, Communications Research Laboratory, for his cooperation in the design and manufacture of the prototype analyzer.

References

1 G. Gloeckler, "Ion composition measurement techniques for space plasmas", Rev. Sci. Instrum., 61, 3613, 1990.

2 K. A. Anderson, R. P. Lin, and H. D. Heetderks, "An experiment to measure interplanetary and solar electrons", IEEE Trans. Geosci. Instrumen., GE-16, 153, 1978.

3 L. A. Frank, D. M. Yeager, H. D. Owens, K. L. Ackerson, and M. L. English, "Quadrispherical LEPDEAS for ISEE7s-1 and -2 plasma measurements", IEEE Trans. Geosci. Electron., GE-16, 221, 1978.

4 S. J. Bame, J. R. Asbridge, H. E. Felthauser, J. P. Glore, G Paschmann, P. Hemmerich, K. Lehmann, and H. Rosenbauer, "ISEE-1 and ISEE-2 fast plasma experiment and the ISEE-1 solar wind experiment", IEEE Trans. Geosci. Instrumen., GE-16, 216, 1978.

5 S. J. Bame, J. R. Asbridge, H. E. Felthauser, J. P. Glore, H. L. Hawk, and J. Chavez, "ISEE-C solar wind plasma experiment", IEEE Trans. Geosci. Instrumen., GE-16, 160, 1978.

6 G. L. Wrenn, J. F. E. Johnson, and J. J. Sojka, "The supra-thermal plasma analyzers on the ESA GEOS satellites", Space Sci. Instrum., 5, 271, 1981.

7 A. J. Coates, J. A. Bowles, R. A. Gowen, B. K. Hancock, A. D. Johnstone, and S. J. Kellock, "The AMPTE UKS three dimentional ion experiment", IEEE Trans. Geosci. Remote Sensing, GE-23, 287, 1985.

8 H. M. Shah, D. S. Hall, and C. P. Chaloner, "The electron experiment on AMPTE UKS", IEEE Trans. Geosci. Remote sensing, GE-23, 293, 1985.

9 A. D. Johnstone, S. J. kellock, A. J. Coates, M. F. Smith, T. Booker, and J. D. Winningham, "A space-borne plasma analyzer for three dimensional measurements of the velocity distribution", IEEE Trans. Nucl. Sci., NS-32, 139, 1985.

10 S. J. Bame, D. J. McComas, B. L. Barraclough, J. L. Phillips, K. J. Sofaly, J. C. Chavez, B. E. Goldstein, and R. K. Sakurai, "The Ulysess solar wind plasma experiment", Astron. Astrophys. Suppl. Sre., 92, 237, 1992.

11 L. A. Frank, K. L. Ackerson, J. A. Lee, M. R. English, and GT. L. Pickett, "The plasma instrumentation for the Galileo mission", Space Sci. Rev., 60, 283, 1992.

12 C. W. Carlson, D. W. Curtis, G. Paschmann, and W. Michael, "An instrument for rapidly measuring plasma distribution functions with high resolution", Adv. Space Sci., 2(7), 67, 1982.

13 M. J. Sablik, D. Golimowski, J. R. Sharber, and J. D. Winningham, "Computer simulation of a 360° field-of-view 'top-hat' electrostatic analyzer", Rev. Sci. Instrum., 59, 146, 1988.

14 T. Mukai, W. Miyake, T. Terasawa, and K. Hirao, "Observations of solar wind ions by the interplanetary spacecraft Suisei (Planet-A)", J. Geomag. Geoelectrc., Vol. 39, 377, 1987.

15 T. Mukai, S. Machida, Y. Saito, M. Hirahara, T. Terasawa, N. Kaya, T. Obara, M. Ejiri, and A. Nishida, "The low energy particle (LEP) experiment onboard the GEOTAIL satellite", J. Geomag. Geoelectrc., Vol. 46, 669, 1994.

16 S. Machida, Y. Saito, Y. Ito, and H. Hayakawa, "Instrument characteristics of the electron spectrum analyzer (ESA) onboard the Planet-B mission and observational perspectives of the electron measurements", Earth Planets Space, Vol. 50, 207, 1998.

17 M. Akioka, K. Ohtaka, T. Nagatsuma, K. Marubashi, and W. Miyake, "L5 Mission and Observation of Interplanetary CME", Journal of the Communications Research Laboratory, Vol. 49, No. 4, 13, 2002.

18 R. P. Lin, K. A. Anderson, S. Ashford, C. Carlson, D. Curtis, E. Ergun, D. Larson, J. McFadden, M. McCrthy, G. K. Parks, H. Reme, J. M. Bosqued, J. Coutelier, F. Cotin, C. D'uston, K. P. Wenzen, T. R. Sanderson, J. Henrion, and J. C. Ronnet, "A three-dimensional plasma and energetic particle investigation for the WIMD spacecraft", Space Sci. Rev., Vol. 71, 125, 1995.

19 W. Miyake and Y. Kazama, "Solar Wind Plasma Instrument for the L5 mission", Journal of the Communications Research Laboratory, Vol. 49, No. 4, 27, 2002.

20 W. Miyake, E. Sagawa, A. Kawabe, and R. Yoshioka, "Calibration System for Charged Particle Analyzer", Review of the Communications Research Laboratory, Vol. 42, No. 2, 245, 1996.(in Japanese)

21 MCP assembly technical report, Hamamatsu Photonics Co., 1991.(in Japanese)

22 J. T. Gosling, J. R. Asbridge, S. J. Bame, and W. C. Feldman, "Effects of a long entrance aperture upon the azimuthal response of spherical section electrostatic analyzers", Rev. Sci. Instrum., 49, 1260, 1978.

23 T. Mukai and W. Miyake, "Transmission characteristics and fringing field effect of a 270° spherical electrostatic analyzer", Rev. Sci. Instrum., 57, 49, 1986.

24 W. C. Feldman and E. Marsch, "Kinetic phenomena in the solar wind", in 'Cosmic winds and the heliosphere', 617, 1997.

25 R. P. Lin, "WIND observations of suprathermal electrons in the interplanetary medium", Space Sci. Rev., Vol. 86, 61, 1998.

26 G. Borrini, J. T. Gosling, S. J. Bame, and W. C. Feldman, "Helium abundance enhancements in the solar wind", J. Geophys. Res., Vol. 87, 7370, 1982.

27 T. H. Zurbuchen, L. A. Fisk, N. A. Schwadron, and G. Gloeckler, "Observations of non-thermal properties of heavy ions in the solar wind", in 'Acceleration and transport of energetic particles observed in the heliosphere: ACE 2000 symposium', 215, 2000.

MIYAKE Wataru, Dr. Sci.

Senior Researcher, Ionosphere and Radio Propagation Group, Applied Research and Standards Department

Space Weather

YAMAZAKI Atsushi, Dr. Sci.

Guest Researcher, Ionosphere and Radio Propagation Group, Applied Research and Standards Department

Earth and Planetary Science